nature biomedical engineering

ARTICLES

https://doi.org/10.1038/s41551-018-0255-5

Spectrally distinct channelrhodopsins for two-colour optogenetic peripheral nerve stimulation

Benjamin E. Maimon[1,2], Kaitlyn Sparks[3], Shriya Srinivasan[1,2], Anthony N. Zorzos[1] and Hugh M. Herr[1]*

Technologies for peripheral nerve stimulation have conventionally relied on the anatomic placement of electrodes adjacent to subsets of sensory fibres or motor fibres that selectively target an end effector. Here, we demonstrate the use of optogenetics to directly target the innervating fibres of an end effector by relying on retrograde transfection of adeno-associated virus serotype 6 to restrict axonal opsin expression to the desired fibre targets. By using an in vivo screen in rats, we identify the first channelrhodopsins as well as a halorhodopsin that respond to red light in the peripheral nerve. Combining two channelrhodopsins with spectrally distinct activation profiles allowed us to drive opposing muscle activity via two-colour illumination of the same mixed nerve. We also show halorhodopsin-mediated reductions in electrically evoked muscle tremor spectrally optimized for deep peripheral nerves. Our non-invasive peripheral neurostimulator with targeted multi-fascicle resolution enables scientific and clinical exploration, such as motor control in paralysis, biomimetic sensation feedback for amputees and targeted inhibition of muscle tremor.

A method for selective stimulation of independent nerve fibre populations within the same nerve in the peripheral nervous system remains a long-sought goal of neural engineers. Peripheral nerves are composed of heterogeneous populations of sensory and motor fibres, intermingled within fascicles, encoding stimuli for both unique anatomical coordinates and functional subgroups of sensory and motor fibres. Nerve fibres that produce the sensation of touch from one side of a finger may travel adjacent to nerve fibres responsible for motor control of a forearm muscle or stretch sensors from a hand muscle. The magnitude of the peripheral nerve (up to 100,000 individual fibres in a single nerve) combined with the difficulty of stimulating individual fibres selectively represents a key impediment to the development and implementation of neural interface technologies for paralysis, pain, amputation, human augmentation and other conditions. Producing a peripheral neural interfacing technology that can selectively and consistently stimulate individual fibre targets with specificity and precision remains an elusive goal.

To date, all techniques employed to tackle this challenge have relied on anatomic targeting of the nerve fibres within fascicles due to their somatotopic organization. Nerve cuff electrodes route current from electrode contact points to the immediately adjacent fibres for spatially distinct stimulation[1]. Longitudinal and transverse intrafascicular electrodes stimulate nerve fibre subpopulations from within the nerve[1–3]. Microchannel and sieve electrodes divide the nerve into distinct regenerated groups, and then stimulate these independently[4]. While great strides have been made in the development and implementation of these technologies, significant challenges remain. Fascicles buried within the nerve are beyond the reach of external multichannel nerve cuff electrical contact points, resulting in inadvertent stimulation of non-targeted fascicles[1]. Both longitudinal and transverse intrafascicular electrodes are not meant for long-term use due to risk of mechanical damage and inflammatory responses within the nerve itself; in addition, both can only target the few fibre groups directly adjacent to the electrode contact points[1]. Regenerated fibres through sieve electrodes do not recapitulate all of the features of healthy nerves, including number and calibre of fibres, functional somatotopic organization and grouping of fibre types within a regenerated channel[5]. Because all of these electrical techniques rely purely on spatial orientation of nerve fibres, they can be difficult to implement consistently in nerves such as the recurrent laryngeal, which has significant mixing of nerve fibres throughout the length of the nerve[6,7]. In addition, all of the techniques above are invasive, requiring implants, which can increase risk of nerve damage. To mitigate the risk of implants, infrared neural stimulation (INS) has been employed to target individual nerves at a distance, which can theoretically achieve high spatial resolution via targeting of unique nerves[8]. However, INS has not been able to stimulate nerve fascicles selectively from a distance, although selectivity was shown invasively using a nerve cuff fixed to an extraneural optical fibre[9]. This is because the INS excitation mechanism is believed to be largely thermal, which increases the difficulty of selective activation of nerve fibre subsets from a distance.

More recently, optogenetic stimulation of the peripheral nerve system has been shown with the translatable goal of mitigating the pathophysiology of several disease states, including chronic pain[10], muscle fatigue[11] and others. One key benefit of the optogenetic approach lies in the selectivity imposed by the viral transfection methodology. Retrograde transfection from a specific injected end effector (for example, muscle, skin) can enable selective stimulation of the nerve fibres that innervate only that specific injection area. Previous efforts have validated end-organ selectivity within muscle tissue by exploring the spatially distinct populations of transfected ventral horn motor neurons within the lumbar spinal cord[12]. Anatomically selective transfection may be a useful method, if applied for the management of chronic pain, paralysis or amputation feedback. However, a method to stimulate two subpopulations independently within the same peripheral nerve distinguished by end effector using optogenetics has proven elusive.

[1]MIT Media Lab, Center for Extreme Bionics, Massachusetts Institute of Technology, Cambridge, MA, USA. [2]Harvard-MIT Program in Health Sciences and Technology (HST), Massachusetts Institute of Technology, Cambridge, MA, USA. [3]Department of Mechanical Engineering, Massachusetts Institute of Technology, Cambridge, MA, USA. *e-mail: hherr@media.mit.edu

One property of the algal channelrhodopsins and halorhodopsins employed for optogenetics lies in the spectrally distinct nature of each opsin. Neuroscientists have sought high-performing red opsins due to the higher transmissivity of red light in biological tissues[13]. Red light can reach neural targets located deeper from the skin surface or through thick neural tissue, which can theoretically activate optogenetic targets with lower surface intensities and attenuate concerns of light-mediated thermal damage[14,15]. Two variants have been identified as exceptionally promising in red-light activation: red-activatiable ChR (ReaChR) and Chrimson, both known to respond in the 600–700 nm wavelength range[16,17]. ReaChR was engineered by replacing the *Volvox* ChR (VChR1) redshifted channelrhodopsin with the N-terminus and L171I point mutation from ChIEF, and the F transmembrane domain from VChR2; the mutations increased photocurrent, wavelength and membrane-trafficking properties, but ReaChR was reported to still suffer from slow channel closure rate $\tau_{1/e} = 137$ ms (ref. [16]). Chrimson was discovered as a naturally occurring opsin in the species *Chlamydomonas noctigama*. Using mutagenesis, Chrimson was engineered into ChrimsonR through the K176R mutation, which further redshifted the opsin's spectrum and shortened $\tau_{1/e}$ from 21.4 ms to 15.8 ms. Whereas ReaChR has previously shown efficacy in mammals in vivo, exploration of Chrimson and ChrimsonR has been limited to brain slices, in vitro neurons and *Drosophila melanogaster* within the published literature[16]. Other redshifted channelrhodopsin variants, including VChR1 and C1V1 have spectral domains that are only slightly shifted from ChR2 with peak excitation wavelengths in the 500–550 nm range[18,19].

When choosing an opsin for peripheral nerve experimentation, wavelength is only one consideration. Other key properties include temporal kinetics to drive tetanic frequencies, photocurrents to decrease depolarization threshold and membrane targeting to drive efficiency of expression. In exploring the diversity of naturally occurring opsins, two other variants are particularly promising: large current channelrhodopsin (CoChR), a powerful blue opsin with 470 nm photocurrents four to five times that of ChR2 (H134R)[20], and *Chloromans subdivsa* ChR (CsChR), an opsin with great membrane trafficking[17]. By taking advantage of CsChR's membrane-trafficking properties, CsChrimson was created from the 74 N-terminus amino acids of CsChR and the 271 transmembrane domain amino acids of Chrimson[17]. CsChrimson has been employed in *Drosophila*, but has not yet been tested in mammals[17]. Spectrally distinct inactivation in peripheral nerve applications is also of significant interest. Jaws, an engineered halorhodopsin with a redshifted inactivation peak at ~600 nm, has been shown to function in the central nervous system, but deep tissue inhibition of peripheral nerve fibres has yet to be explored[21].

Independent two-colour neuronal stimulation was shown in brain slices following in utero electroporation with both ChrimsonR and CoChR[17]. However, when applying the best potential opsin candidates within the optogenetics toolbox to the peripheral nervous system, several system-specific challenges arise. First, the efficacy of viral transfection is significantly lower in the peripheral nervous system compared with the central nervous system due to the low efficiency of retrograde viral transfection of adeno-associated virus (AAV)[22]. Second, the peripheral nervous system is not immune-protected like much of the central nervous system. Immune responses to intramuscular injections have been shown for AAV injections in several mammalian species including humans for a variety of AAV-mediated gene transfection applications[23,24]. Third, expression of opsin protein localized to the cell body of the neuron is not sufficient to induce optogenetic responses to peripheral nerve illumination. Murine peripheral nerves can extend ~20 cm in length, compared with the ~30 μm neuronal cell diameter. Previous mapping of neurons in the central nervous system in transgenic mice has suggested that direct illumination of the axon itself may not be sufficient to induce an action potential, compared with direct illumination of the cell body[25]. Successful nerve transfection implies sufficient opsin expression within the entire length of the axon membrane such that illumination anywhere along the nerve produces an action potential. These challenges significantly increase the difficulty of peripheral nerve optogenetics implementations compared with those of the central nervous system.

An analysis of promising opsins specific to the peripheral nerve would confer an enormous benefit to future scientific studies as well as a framework for future translatable systems for optogenetic disease treatment. We hypothesize that the intramuscular injection of AAV serotype 6 (AAV6) coding for a red opsin and a blue opsin in opposing muscle pairs would enable selective transfection of the nerve fibres corresponding to each muscle via spectrally distinct illumination of the same mixed nerve. We evaluate this hypothesis by screening several opsins with unique properties in the peripheral nervous system, and then applying the most promising, spectrally distinct candidates together in opposing muscle subsets of a rat hindlimb in vivo as a function of both modelled and applied fluence rate.

Results

Optogenetic peripheral nerve expression is opsin dependent. Of the six channelrhodopsins evaluated, four (ReaChR, CoChR, CsChrimson and ChR2) resulted in successful electrophysiological muscle expression in response to illumination of the nerve. As expected, all four opsins exhibited electromyography (EMG) spikes in response to 473 nm illumination, but only ReaChR and CsChrimson exhibited spikes in response to 635 nm illumination (Fig. 1c). Unexpectedly, the strength of the EMG response to 473 nm illumination was greatest in ChR2 as measured in both the tibialis anterior (TA) and gastrocnemius (GN) channels, despite the higher photocurrents of CoChR[17] (Fig. 1d). Within the red channel, we found that the strength of the CsChrimson EMG in response to 635 nm illumination greatly exceeded that of ReaChR (Fig. 1d). Despite multiple attempts, transdermal or direct illumination of the exposed sciatic nerve of animals injected with either Chrimson or ChrimsonR at 473 nm or 635 nm did not result in any electrophysiological spiking at any time during the course of the experiment (Fig. 1c). Additional in vivo ChrimsonR experiments varying virus source, dosage, age of injection, serotype and injection volume surprisingly did not produce any electrophysiological twitches at any time (Supplementary Fig. 6a), despite verified in vitro expression of the opsin measured both with fluorescence (Supplementary Fig. 7g) and with patching (Supplementary Fig. 6b,c). Force and EMG were found to be linearly related within the range of EMG and force measurements produced by optogenetic activity (Supplementary Fig. 1b), in line with previous findings[26].

We identified a key differential in the optical sensitivity for both CsChrimson and ReaChR as a function of illumination intensity (Fig. 1e). At low illumination intensities (2.8 mW mm^{-2}), 635 nm illumination produced strong CsChrimson EMG comprising many distinct motor units. However, 635 nm illumination could not elicit ReaChR EMG until the illumination intensity exceeded 25 mW mm^{-2}. Conversely, 473 nm illumination resulted in ReaChR EMG at low illumination intensities (2.8 mW mm^{-2}), but CsChrimson required at least 16 mW mm^{-2} for weak stimulation. Despite robust stimulation of ReaChR at a range of wavelengths, CsChrimson remained the only opsin identified to have higher sensitivity to red light compared with blue light, making it a prime candidate for two-colour peripheral nerve optogenetics.

The frequency response of each opsin in the peripheral nerve was found to be in agreement with previously reported in vitro characterizations[16,17]. ReaChR was not able to sustain high-frequency firings over 5 Hz. The frequency producing the maximum root-mean-square voltage (V_{RMS}), f_{max}, was identified for CsChrimson,

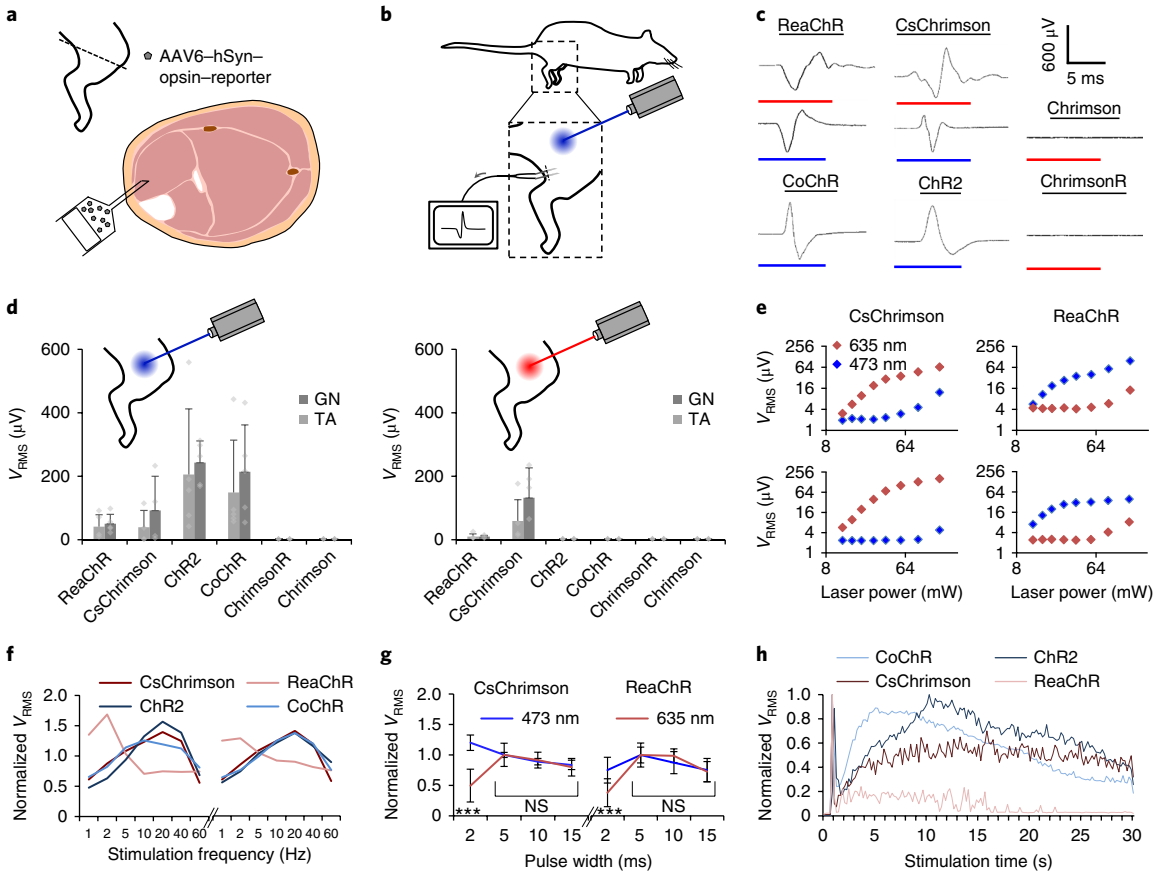

Fig. 1 | Comparison of channelrhodopsin activity in the peripheral nerve. a, AAV6–hSyn–opsin–reporter injected into anterior compartment of Fischer 344 rats 2 days postpartum. **b**, At 2, 4, 6 and 8 weeks post-injection, a 473 nm laser (shown) or 635 nm laser (not shown) illuminated surface of animal while EMG was recorded. **c**, Selected EMG spikes from optogenetic activation with either 473 nm pulses (blue) or 635 nm pulses (red). **d**, V_{RMS} mean ± s.d. calculated from 45 mW mm^{-2} illumination of exposed sciatic nerve at 4 weeks post-injection for 473 nm (left) and 635 nm (right) illumination recorded from the TA and GN muscles. $n = 5$ biologically independent animals for each group except $n_{CsChrimson} = 4$. Laser pulse width = 10 ms and frequency = 5 Hz. **e**, Comparison of 473 nm and 635 nm GN V_{RMS} induced by direct illumination of exposed sciatic nerve varying illumination intensities for two CsChrimson (left) and two ReaChR (right) rats 4 weeks post-injection. **f**, Normalized V_{RMS} mean as a function of stimulation frequency for 473 nm illumination of exposed sciatic nerve 4 weeks post-injection for both GN (left) and TA (right). $n = 5$ biologically independent animals for each group except $n_{CsChrimson} = 2$ and $n_{ReaChR} = 4$. Laser pulse width = 10 ms and intensity = 45 mW mm^{-2}. **g**, Normalized V_{RMS} mean ± s.d. as a function of stimulation pulse width for 473 nm and 635 nm illumination of both transdermal and exposed nerve trials. V_{RMS} calculated for each trial with a minimum threshold set to 3.25 μV to exclude noise, normalizing across all pulse widths for each animal and then averaging all trials. n represents the biologically independent experiments where V_{RMS} exceeded the minimum threshold: $n_{CsChrimson473} = 7$, $n_{CsChrimson635} = 40$, $n_{ReaChR473} = 34$, $n_{ReaChR635} = 11$. Laser frequency = 5 Hz and intensity = 45 mW mm^{-2}. Comparison was performed using Student's two-tailed t-test with unequal variance. ***$P < 0.001$; $P_{CsChrimson,2ms} = 1\times10^{-8}$; $P_{ReaChR,2ms} = 4\times10^{-5}$. NS, not significant. **h**, Representative rolling average V_{RMS} from each animal at 4 weeks in response to direct illumination of the nerve with 473 nm light (CoChR, ReaChR, ChR2) or 635 nm light (CsChrimson) for 30 s at 40 Hz and 10 ms pulse width, normalized to maximum EMG over 30 s.

ChR2 and CoChR to be 20 Hz. For ReaChR, $f_{max} = 2$ Hz (Fig. 1f). CsChrimson was also found to have a slight peak shift with 635 nm illumination to $f_{max} = 10$ Hz compared with 473 nm illumination (Supplementary Fig. 8a). Unlike the frequency response, the pulse width response was found to be similar for all four opsins for 473 nm stimulation (Supplementary Fig. 8b). Although the strength of the response appeared to decrease with increasing pulse width, this was likely indicative of low recovery time between stimulation trains and was not indicative of a physiologic phenomenon. However, for both CsChrimson and ReaChR, the strength of the EMG in response to a 2 ms pulse width of 635 nm illumination was significantly lower than in response to a 2 ms pulse of 473 nm illumination (Fig. 1g), indicating that opsin on-kinetics are wavelength dependent. To evaluate each opsin's response to a prolonged stimulation train, a 30 s step response to 40 Hz stimulation was measured. Normalized V_{RMS} showed nonlinearity for all opsins (Fig. 1h). A rapid, strong peak corresponding to the onset of illumination was followed by an ~2 s refractory period where muscle activity dropped sharply. A 2–10 s V_{RMS} recovery generally followed until a slow, steady decline of muscle activity due to fatigue until stimulation ended. Due to its slow off-kinetics, ReaChR was constrained to a strong initial peak followed by a dearth of follow-up activity. The approximate shape of the step response was bucketed for each opsin and trial, revealing that ChR2 and CoChR were consistently activated throughout the full illumination duration compared with CsChrimson and ReaChR, which showed weaker activity following the initial pulse (Supplementary Fig. 8c).

High EMG efficiency suggests ChR2 is most robust opsin for peripheral nerve stimulation. The electrophysiological results aligned well with histological findings. Sciatic nerve cross-sections of each opsin revealed strong expression for ReaChR, CsChrimson,

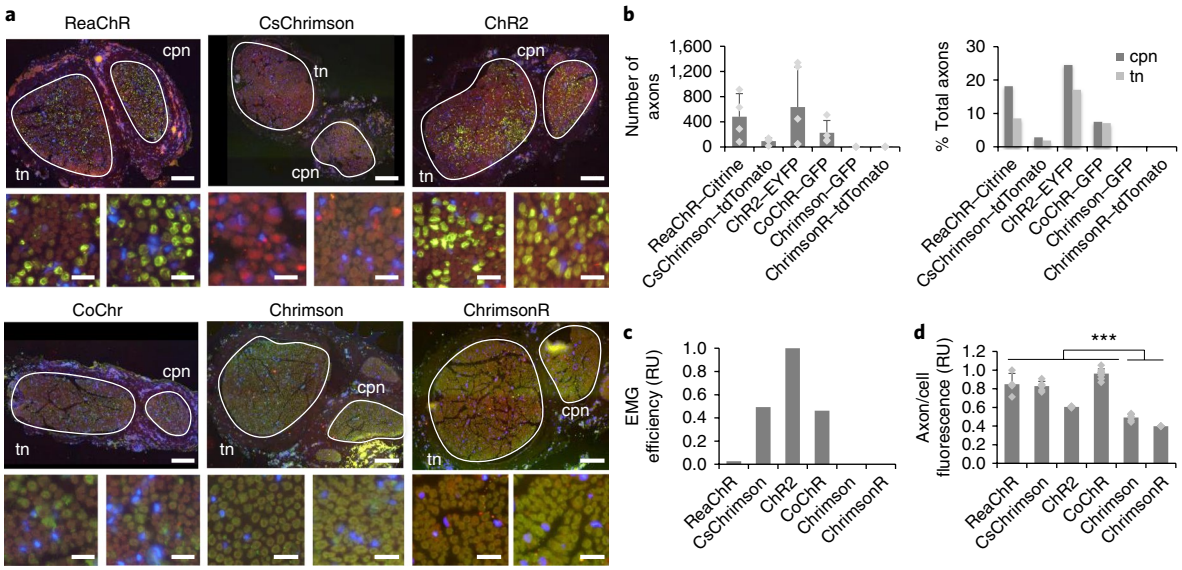

Fig. 2 | Comparison of channelrhodopsin expression in the peripheral nerve. a, Top images: sciatic nerve stained for GFP, EYFP or Citrine (green), tdTomato (red) and DAPI (blue) with outlined divisions for common peroneal nerve (cpn) and tibial nerve (tn). Scale bars, 150 µm. Bottom images: representative zoom in sections of tn (left) and cpn (right). Experiment was repeated three times with similar results for ReaChR, CsChrimson and CoChr, and experiment was repeated four times with similar results for ChR2, Chrimson and ChrimsonR. Scale bars, 15 µm. **b**, Opsin$^+$ axons in sciatic nerve section mean ± s.d. (left) and as a percentage of total counts in representative cpn and tn fascicles (right). **c**, EMG efficiency calculated as GN V_{RMS} of 8-week-old rat to 473 nm illumination (ReaChR, ChR2, CoChR) or 635 nm illumination (CsChrimson) on exposed sciatic nerve divided by number of opsin$^+$ axons in highest expressing rat of each group (45 mW mm^{-2}, 5 Hz, 10 ms). **d**, Ratio of in vitro fluorescence of axon to cell body for ChR2 ($n = 6$), CoChR ($n = 10$), CsChrimson ($n = 7$), ReaChR ($n = 4$), ChrimsonR ($n = 4$) and Chrimson ($n = 7$), where n is the number of biologically independent cells. Comparison was performed using Student's two-tailed t-test with unequal variance. ***$P < 0.001$; $P = 5 \times 10^{-13}$.

ChR2 and CoChR compared with Chrimson and ChrimsonR (Fig. 2a). ReaChR animals 2 and 3 showed robust axon immunofluorescence and CsChrimson animals 1 and 5 showed moderate immunofluorescence compared with other animals in those same groups, aligning identically with the presence of EMG from direct sciatic nerve illumination of those same animals just before euthanasia (Figs. 2b and 5a). For each electrophysiologically active opsin, an EMG efficiency was calculated from the ratio of V_{RMS} to total opsin + axon counts (Fig. 2c). Although ReaChR had high axonal expression, it produced weak action potentials, resulting in low opsin efficiency. CsChrimson, despite having low axon counts, produced reasonable EMG signals resulting in a stronger efficiency. Despite the high photocurrents of CoChR, ChR2 had the highest efficiency, producing very high EMG signals compared with its histological fluorescence counts.

Despite lack of in vivo immunofluorescent or EMG responses for Chrimson and ChrimsonR, we discovered in vitro fluorescence in all opsins in hippocampal cultures (Supplementary Fig. 7). Expression in the cell body was much higher than in the axonal projections for each opsin. The ratio of axonal expression to cell body expression was calculated, normalized and compared across opsins (Fig. 2d). Notably, ChrimsonR and Chrimson demonstrated ratios (<0.5) that were significantly smaller than the other opsins, suggesting expression was more concentrated in the cell body for these opsins. Spinal cord immunofluorescence revealed clear, ipsilateral opsin$^+$ expression in ventral horn neurons for all opsins except for Chrimson and ChrimsonR, which may have had some very weak expression compared with the contralateral side (Supplementary Fig. 9a). These results together suggest that the lack of Chrimson and ChrimsonR expression within motor axons may be related to both overall low levels of cytoplasmic protein as well as poor axonal membrane trafficking.

CsChrimson and ChR2 drive two-colour independent stimulation of subsets of sciatic nerve. After characterizing the individual opsins, three P14 rats and six P2 rats were injected with AAV6 carefully targeting the TA for CsChrimson and the GN for ChR2 (Fig. 3a). For the P2 rats, transdermal illumination 4 weeks post-injection provided both dorsiflexion and TA spikes in response to red light compared with plantarflexion and GN spikes in response to blue light (Fig. 3b); these movements and electrical recordings were repeatable even when the light-source position on the surface of the skin was reversed (Supplementary Video 1), demonstrating source-agnostic control of peripheral nerve subsets. At 8 weeks post-injection, the sciatic, peroneal and tibial nerves were exposed. Illumination of the peroneal nerve exclusively revealed EMG spikes in the TA EMG channel. The 635 nm illumination elicited a very strong V_{RMS} response as low as 10 mW (2.8 mW mm^{-2}), whereas the 473 nm illumination could only produce spikes at 160 mW (45 mW mm^{-2}; Fig. 3d), consistent with the illumination intensity recruitment curve for CsChrimson (Fig. 1e). Conversely, illumination of the tibial nerve exclusively revealed EMG spikes in the GN channel only, and only in response to 473 nm illumination (Fig. 3d), consistent with the illumination intensity recruitment curve for ChR2[15].

Direct illumination of the exposed sciatic nerve with blue and red light produced EMG specific to the injected muscle (Fig. 3c,e and Supplementary Video 1). Co-stimulation of both muscles with blue and red illumination produced co-contraction. The TA channel EMG increased slightly with co-stimulation compared with red illumination alone, indicating that blue illumination recruited additional CsChrimson motor units, which were subthreshold with red illumination. However, red illumination did not influence the strength of the GN channel, consistent with the inability of ChR2 to be activated by red illumination. Independent two-colour EMG was also seen via transdermal illumination of the sciatic nerve

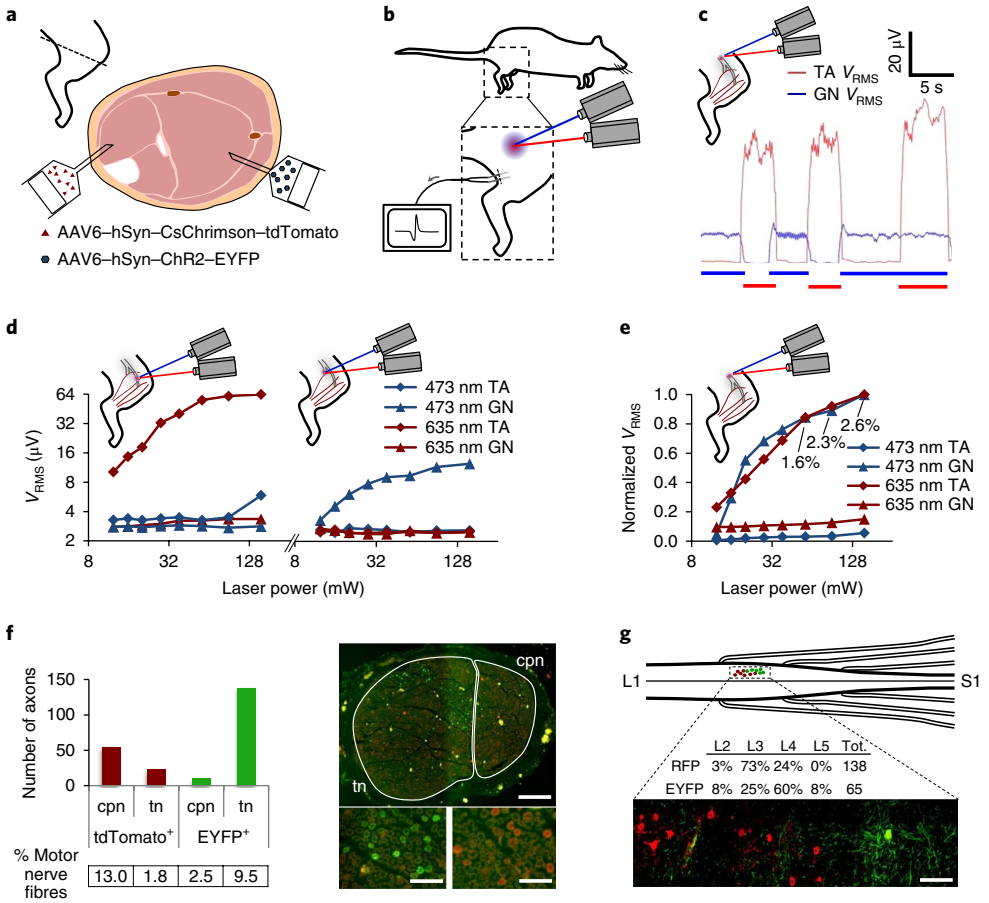

Fig. 3 | Optogenetic activation with two unique wavelengths drives opposing ankle movements. a, CsChrimson and ChR2 injected into anterior and posterior compartments of P2 or P14 Fischer 344 rat. **b**, After 4 and/or 8 weeks, 473 nm and 635 nm lasers illuminated the exposed nerves while EMG was recorded. **c**, Moving average V_{RMS} elicited by co-localized 635 nm laser (red) and 473 nm laser (blue) directly illuminating exposed sciatic nerve. Lasers differentially activate TA (red) and GN (blue) electrodes (5 Hz, 3 ms pulse width, intensity $I_{635nm} = 45\,mW\,mm^{-2}$, $I_{473nm} = 25\,mW\,mm^{-2}$; V_{RMS} calculated every 0.1 s with 0.5 s window). **d**, With both lasers co-localized on the common peroneal nerve (cpn, left) and tibial nerve (tn, right), the 473 nm laser, followed by the 635 nm laser, was ramped in a power sweep from 12 to 160 mW while TA and GN EMG were recorded (5 Hz, 10 ms pulse width, 4 s each). Experiment repeated two times with similar results. **e**, With both lasers co-localized on the sciatic nerve, the 473 nm laser, followed by the 635 nm laser was ramped in a power sweep from 12 to 160 mW while TA and GN EMG were recorded (5 Hz, 10 ms pulse width, 4 s each). EMG was normalized to maximum V_{RMS} for each wavelength. Force is also shown as a percentage of body weight, at the illumination intensities where force exceeded the recordable threshold. Experiment repeated two times with similar results. **f**, Immunolabelling reveals spatially distinct opsin within tn and cpn fascicles of the mixed sciatic nerve in both absolute and relative quantities depicting tdTomato (red) and EYFP (green). Scale bars: top, 200 μm; bottom, 25 μm. Experiment repeated once with similar results. **g**, Spinal cord histological section showing tdTomato$^+$ neurons (CsChrimson) and EYFP$^+$ neurons (ChR2$^+$) generally in distinct groups, corresponding to their relative ventral horn locations. (L1 = lumbar vertebra 1; S1 = sacral vertebra 1; RFP = red fluorescent protein = tdTomato). Scale bar, 250 μm. Counts by lumbar vertebra summed and displayed as percentages and absolute totals (Tot.) with RFP = tdTomato. Experiment repeated once with similar results.

using high-powered light-emitting diodes (LEDs) (Supplementary Fig. 10 and Supplementary Video 1). Electrophysiological findings are consistent with histologic evaluation of the mixed sciatic nerve's tibial and peroneal fascicles, which contained seven times more ChR2$^+$ axons and six times more CsChrimson$^+$ axons, respectively (Fig. 3f). The unexpected presence of some tdTomato$^+$ axons in the tibial nerve (1.8%) and some enhanced yellow fluorescent protein (EYFP)$^+$ axons in the peroneal nerve (2.5%) may be due to viral spread at the time of injection at the level of the nerve and/or muscle. The overall percentage of myelinated axons transduced remained low at ~5% for the peroneal nerve (16% of peroneal motor axons) and ~2.5% for the tibial nerve (12% of tibial motor axons), consistent with histology for CsChrimson alone[27]. Coronal cross-sections of the spinal cord showed spatial distinction of the predominately cranially located CsChrimson$^+$ neurons compared with caudally located ChR2$^+$ neurons (Fig. 3g), consistent with rat studies of spinal anatomy[28,29]. tdTomato$^+$ neurons were predominantly located in lumbar vertebra 3 (L3) (73%) whereas EYFP$^+$ neurons were predominantly located in L4 (60%). Presence of transduced neurons in non-target regions is likely due to viral spread. Axial spinal cord cross-sections at the L3/L4 border revealed distinct groupings of CsChrimson$^+$ and ChR2$^+$ neurons within the ipsilateral ventral horn (Supplementary Fig. 9b). Taken with the electrophysiological results, these histological findings validate independent transduction and optogenetic stimulation of subsets of peripheral nerve targets.

Fourfold higher fluence rate for deep nerves with 635 nm illumination. To evaluate how much farther red light can penetrate in deep tissue peripheral nerve targets, a Monte Carlo model was

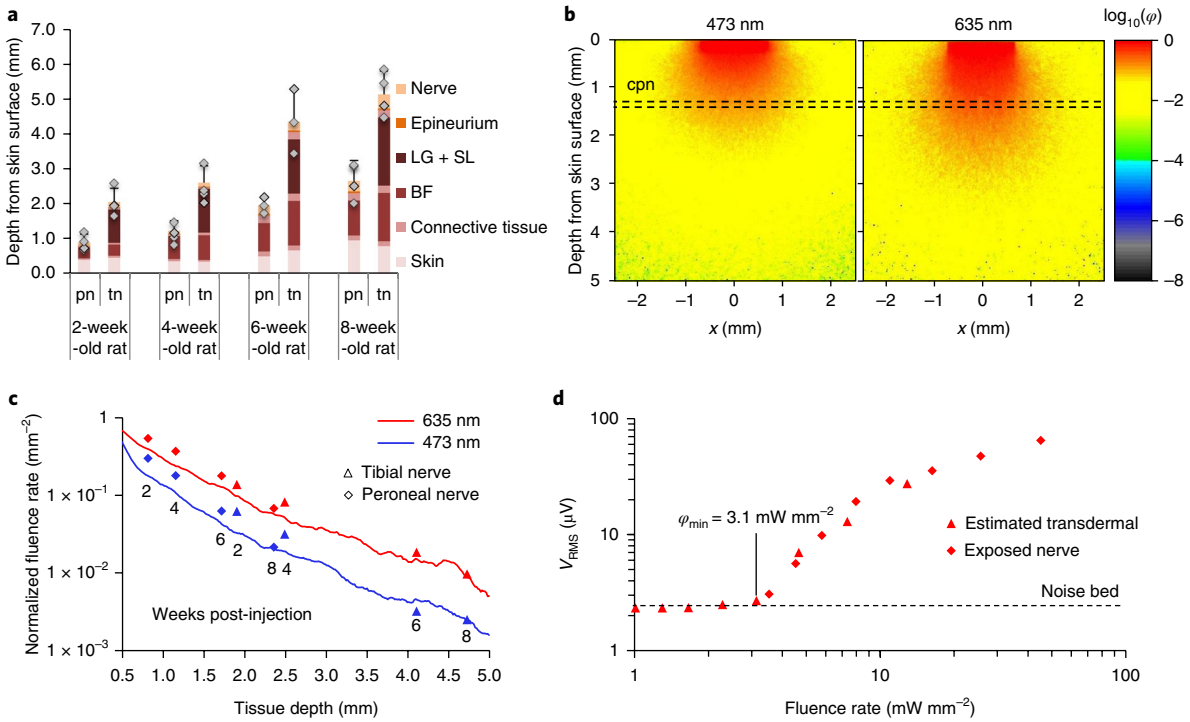

Fig. 4 | Fluence rate modelling reveals moderately increased levels of red light within deeper tissues. a, Tissue depth mean ± s.d. representing distance from skin surface to nerve at most superficial location for peroneal nerve (pn) and tibial nerve (tn). For each reported geometry, $n = 4$ biologically independent animals except for 6-week-old rats where $n = 3$ biologically independent animals. LG, lateral gastrocnemius; SL, soleus; BF, biceps femoris. **b**, Two-dimensional representation of 473 nm and 635 nm Monte Carlo output with common peroneal nerve (cpn) location shown for 4-week-old pn geometry with φ = normalized fluence rate and and x = radial distance from beam centre. **c**, Monte Carlo output with fluence rate along centreline for modelled 8-week-old tn for both 635 nm and 473 nm illumination along with independently modelled Monte Carlo for pn and tn for 2-, 4-, 6- and 8-week-old cpn and tn. **d**, Measured GN EMG as a function of fluence rate for both transdermal 635 nm illumination of tn (estimated fluence rate from Monte Carlo model) and direct stimulation of exposed sciatic nerve (known fluence rate) of same CsChrimson$^+$ nerve at 4 weeks post-injection.

constructed for the full range of tissue geometries analysed in this study. Tissue cross-sections revealed a nerve depth ranging from 0.8 mm for the 2-week-old peroneal nerve to 5.0 mm for the 8-week-old tibial nerve (Fig. 4a) with the majority of the intermediate tissue represented by skin and muscle (Supplementary Fig. 4). The Monte Carlo model showed the fluence rates from 635 nm illumination well exceeded fluence rates from 473 nm illumination for all nerves modelled. Whereas the $\log_{10}$ reduction of normalized blue light fluence rate is constrained to the first ~1 mm of tissue, the equivalent red light permeated approximately ~2 mm, within range of the 2-week-old tibial nerve (Fig. 4b). The Monte Carlo model showed that at depth, blue light was more targeted than red light, consistent with transdermal findings; whereas red illumination of the mid-calf targeting the tibial nerve elicited both strong GN and TA responses, blue illumination excited more GN activity (Supplementary Fig. 8d). A centreline plot showing fluence rate as a function of tissue depth revealed that blue fluence rate exceeded red fluence within the first ~300 μm of tissue, consistent with the increased anisotropy of the scattering of red light compared with blue light (Fig. 4c). After the crossing point, red fluence gradually increased relative to blue fluence, reaching approximately four times greater by a 4 mm depth.

The normalized fluence rate to 635 nm illumination was found to be 6.8×10^{-2} mm^{-2} at the peroneal nerve for the 8-week-old rat and 9.7×10^{-3} mm^{-2} at the tibial nerve of the 8-week-old rat (Fig. 4c). As such, the 160 mW, 635 nm laser source, transdermally incident, yielded fluence rates of 10.9 mW mm^{-2} and 1.6 mW mm^{-2} at each of the respective nerves. Comparatively, the normalized fluence rate to 473 nm illumination was found to be 2.1×10^{-2} mm^{-2} at the peroneal nerve and 2.5×10^{-3} mm^{-2} at the tibial nerve, showing a three- to fourfold difference. An EMG versus fluence rate comparison between transdermal illumination (subject to the Monte Carlo results) and direct illumination of the exposed nerve showed V_{RMS} agreement within the overlap range, suggesting the Monte Carlo model accurately predicted fluence rate at the nerve (Fig. 4d). A thermal analysis using incident irradiation showed a maximum temperature increase of 1.16 °C for 473 nm and 1.05 °C for 635 nm at the two-week-old peroneal nerve (Supplementary Fig. 5a,b). For both wavelengths, the heat dissipated by ~35% within 0.5 s of ending stimulation. The model was found to reach steady state at ~7 s (Supplementary Fig. 5c), suggesting that pulsed 30 s illumination, even directly on the exposed nerve, would be the subthreshold for heating-induced optical nerve activity, which is primarily dependent on a threshold nerve temperature of 42–45 °C (ref. [30]).

ChR2 outperformed CoChR, ReaChR and CsChrimson despite elevated red fluence rates at depth. When comparing all opsins, peak optogenetic excitability was found 4 weeks post-injection as measured by number of animals responding to illumination (Fig. 5a), consistent with our previously reported loss of optogenetic responsiveness from 5 weeks to 8 weeks post-injection for ChR2[15]. At 4 weeks, 5/5 ReaChR and 5/5 CsChrimson animals responded to 160 mW transdermal illumination of blue and red light, corresponding to Monte Carlo-modelled fluence rates of 1.9 mW mm^{-2} and 3.8 mW mm^{-2} at the peroneal nerve surface, respectively. At 8 weeks, however, 0/5 ReaChR and 0/4 CsChrimson animals responded to transdermal illumination of either wavelength. Direct illumination of the exposed nerve activated 2/5 ReaChR and 2/4 CsChrimson animals, respectively, at minimum fluence rates of

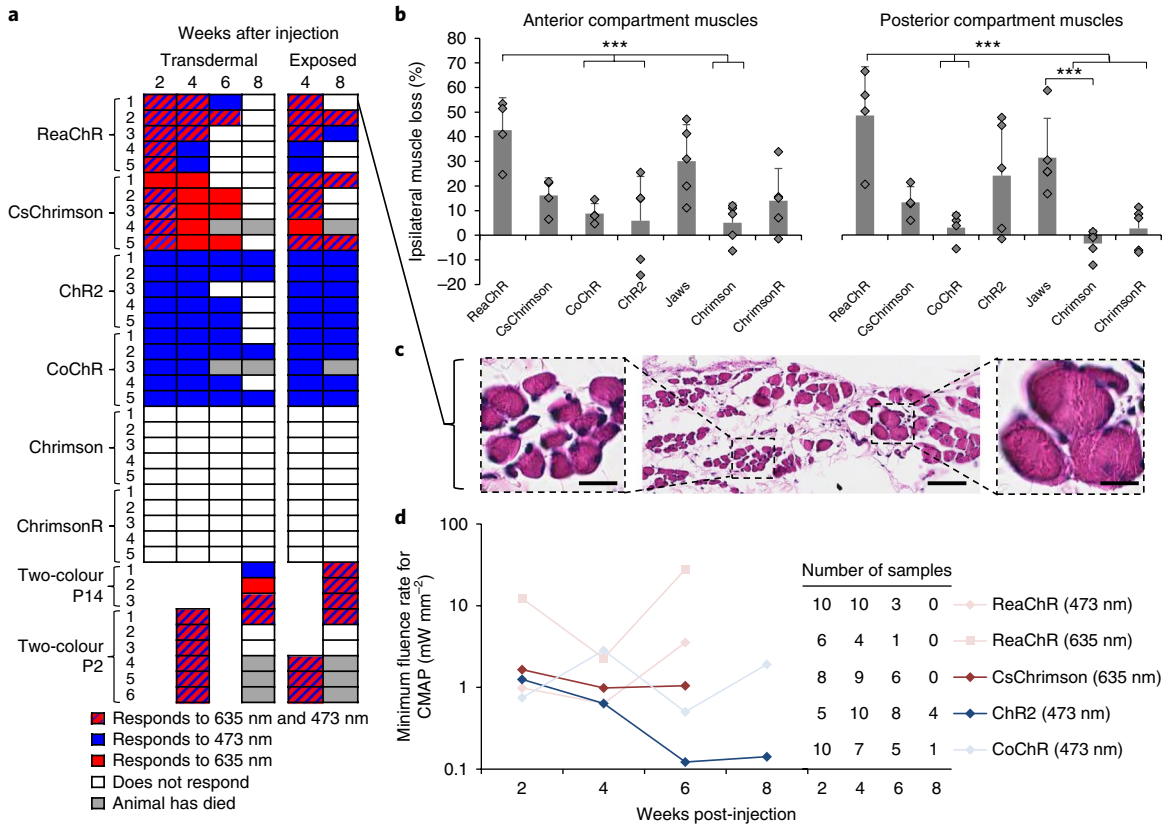

Fig. 5 | Loss of expression is opsin dependent with highly expressing nerves requiring low fluence rates for activation. a, Excitability to blue and red illumination in both transdermal (left) and exposed nerve (right) as a function of weeks post-injection for each animal tested. **b**, Anterior compartment muscle atrophy mean ± s.d. as a percentage decrease from contralateral side (left); posterior compartment muscle atrophy mean ± s.d. as a percentage decrease from contralateral side (right). $n = 4$ biologically independent animals for ReaChR, CsChrimson and CoChR and $n = 5$ biologically independent animals for ChR2, Jaws, Chrimson and ChrimsonR. Comparison performed using one-factor ANOVA and Fishers two-tailed least significance difference post-hoc test. $^{***}P < 0.001$; $P_{Anterior} = 9 \times 10^{-4}$; $P_{Posterior} = 9 \times 10^{-5}$. **c**, H&E cross-section of TA of ReaChR animal (centre; scale bar, 80 μm) with breakout (left/right; scale bars, 20 μm). Experiment repeated three times with similar results. **d**, Minimum fluence rate for compound muscle action potential (CMAP) calculated by multiplying minimum illumination power to produce each animal's transdermal EMG spike by the estimated fluence rate for that animal and wavelength from Fig. 4d. Sample sizes for each group shown.

16 mW mm^{-2}, strongly suggesting loss of expression over time as opposed to losses due to anatomic changes alone. CoChR and ChR2 animals fared slightly better with 2/4 and 2/5 animals, respectively, maintaining responsiveness to transdermal blue illumination at 8 weeks. In addition, all of the ChR2 and CoChR animals maintained optogenetic excitability to direct stimulation of the sciatic nerve at 8 weeks post-injection, although this EMG response was weak for certain animals.

Ipsilateral muscle mass reductions were noted in most opsin-expressing groups; loss of optogenetic responsiveness appeared to correlate with muscle atrophy by opsin group (Fig. 5b). The ReaChR animals exhibited the most significant reductions (40–50%) in muscle mass for both anterior and posterior compartments, significantly greater than CoChR and Chrimson groups. Jaws animals also had muscle mass reductions in both anterior and posterior compartments of ~30%. CsChrimson and ChR2 had moderate muscle mass losses ranging from 10 to 25% for both groups. Chrimson and ChrimsonR never expressed optogenetically, so the lack of ipsilateral muscle loss correlated with lack of expression. CoChR, which still expressed fairly well at 8 weeks post-injection, had negligible muscle loss as well. Haemotoxylin and eosin (H&E) cross-sections of the TA revealed shrunken myocytes (Fig. 5c, left) interspersed within fibrous tissue and healthy myocytes (Fig. 5c, right), characteristic of denervation atrophy. Despite the atrophy, there were no obvious signs of immune cells or inflammatory infiltrates directly within the muscle. However, coronal H&E sections of spinal cord suggest increased presence of inflammatory cells adjacent to opsin-expressing motor neurons (Supplementary Fig. 9c), in agreement with previously reported elevated cellularity[15]. Further, spinal cord sections show as high as a 46 ± 13% ipsilateral ventral horn motor neuron loss, which was identified in the ReaChR rats. CsChrimson, ChR2 and CoChR all had neuronal losses of ~30%. Chrimson and ChrimsonR did not have any significant neuronal losses (Supplementary Fig. 9c). Lastly, the presence of ipsilateral inflammation, as defined by density of cells within ventral horn, was identified in a similar pattern, with ReaChR having the highest measured inflammation (40% increase of ipsilateral cell counts) and Chrimson/ChrimsonR having no significant increase in ipsilateral cell counts (Supplementary Fig. 9d). Together, these findings suggest that neuronal death of specifically opsin + neurons is leading to loss of optogenetic peripheral nerve expression along with an accompanying denervation muscle atrophy at the target muscle.

The minimum transdermal illumination for spike induction was mapped via the Monte Carlo estimated fluence rates to provide a minimum nerve fluence rate capable of eliciting action potentials for each opsin (Fig. 5d); these numbers account for both the increased fluence of red light at depth as well as each rat's growth over the experimental period. For all opsins, the minimum fluence rate was

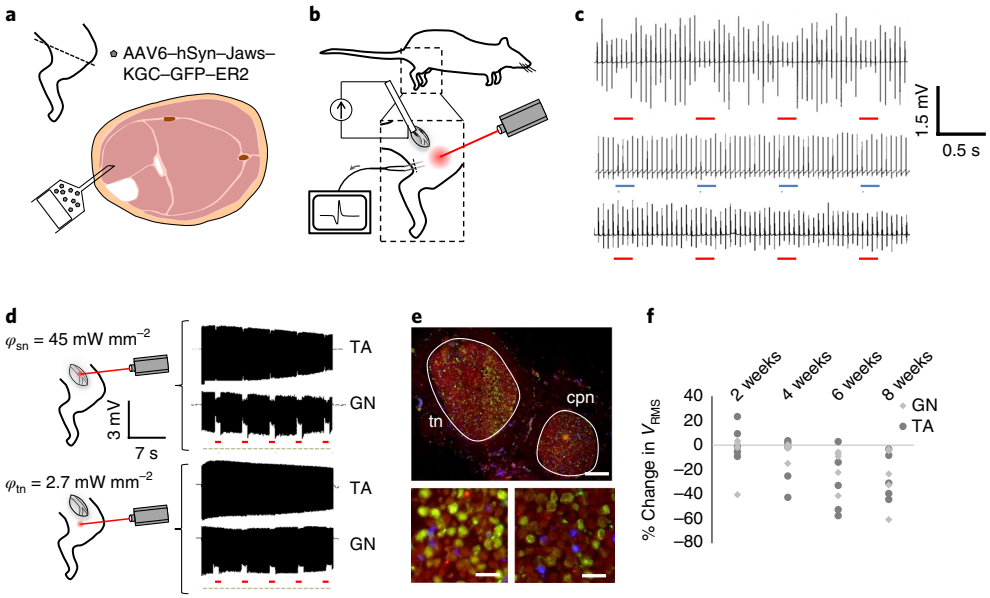

Fig. 6 | Jaws inhibits motor activity. a, AAV6-hSyn-Jaws-KGC-GFP-ER2 (15 µl) targeting anterior compartment of Fischer 344 rats 2 days postpartum. **b**, At 2, 4, 6 and 8 weeks post-injection, a current-controlled hook electrode stimulated the exposed sciatic nerve while concurrent 635 nm laser illumination was directed either transdermal to the TA or GN motor points or the exposed sciatic nerve. **c**, GN EMG traces from 16 Hz, 50 µs supramaximal electrical stimulation of sciatic nerve of 8-week-old rat with 635 nm laser illuminating ipsilateral sciatic nerve (top; $n=5$ biologically independent animals), 473 nm laser illuminating ipsilateral sciatic nerve (middle; $n=2$ biologically independent animals) and 635 nm laser illuminating contralateral sciatic nerve (bottom, $n=5$ biologically independent animals). **d**, Comparison of optogenetic-induced peak-peak voltage (V_{pp}) reductions in 2-week-old animal with direct illumination of exposed sciatic nerve (top) and transdermal illumination of GN motor point (bottom). Estimated maximum tibial (φ_{tn}) and sciatic nerve surface fluence rates (φ_{sn}) shown ($n=2$ biologically independent animals). **e**, Sciatic nerve cross-section showing Jaws expression in both tibial nerve (tn) and common peroneal nerve (cpn). Experiment repeated four times with similar results. **f**, Percent reduction in V_{RMS} between laser on and laser off calculated by $(V_{RMS,LaserOn} - V_{RMS,LaserOff})/V_{RMS,LaserOff}$ ($n=5$ biologically independent animals for both GN and TA).

found between 4 and 6 weeks post-injection, consistent with previously reported loss of excitability of the best-expressing axons over time. Of all opsins, ChR2 required the lowest overall fluence to initiate action potentials of 122 µW mm^{-2}, roughly four times smaller than CoChR's minimum of 502 µW mm^{-2}. Comparatively, CsChrimson (635 nm) and ReaChR (473 nm) had higher minimum fluence rates of 984 µW mm^{-2} and 636 µW mm^{-2}, respectively, both at 4 weeks post-injection. ReaChR's responsiveness to 635 nm illumination as measured by minimum fluence was three- to tenfold greater than its responsiveness to 473 nm illumination at measured ages, aligning with the ReaChR's higher V_{RMS} sensitivity to 473 nm illumination.

Jaws inhibits muscle tremor in wavelength-dependent manner. To assess motor inhibition using Jaws, supramaximal current was delivered directly to the sciatic nerve via a hook electrode at 17 Hz and 50 µs pulse width (Fig. 6b). The 635 nm illumination (160 mW, 1 Hz, 20% DC) on the exposed sciatic nerve resulted in consistent attenuation in the measured EMG at the downstream muscles (Supplementary Video 1 and Fig. 6c, top). The 473 nm illumination of the same nerve had little to no effect on the measured EMG (Fig. 6c, middle), consistent with both the higher scattering of blue light and the higher relative sensitivity of Jaws to red illumination[21]. Two strategies verified that the tremor reduction during illumination was optogenetic and not thermal. First, 635 nm illumination of the contralateral sciatic nerve with identical functional electrical stimulation (FES) produced no measureable changes in EMG (Fig. 6c, bottom). Second, a thermal analysis found that limiting the duty cycle to 20% limited the maximum temperature increase in the tissue to 0.82 °C following 10 s of stimulation, well below the temperature limit for thermally mediated nerve firing effects[30] (Supplementary Fig. 5d).

Jaws motor inhibition was not limited to direct illumination of the exposed sciatic nerve. Notably, ~15% EMG reduction was achieved with transdermal illumination targeting the tibial nerve, compared with ~50% EMG reduction with 1 s of 635 nm pulses directly on the sciatic nerve (Fig. 6d) consistent with the modelled reduction in nerve surface fluence rates. In addition, the small TA EMG reductions associated with stimulation of the sciatic nerve directly disappeared completely with illumination targeting the tibial nerve, suggesting spatial selectivity of transdermal inhibition. Histological evaluation of Jaws sciatic nerve cross-sections revealed similar findings to channelrhodopsins, with consistent expression in ~15% axons (Fig. 6e). Not all animals resulted in a strong reduction in FES-induced tremor. Maximum tremor reduction as measured by V_{RMS} was ~60%, achieved at 6 and 8 weeks post-injection (Fig. 6f).

Discussion

In this experiment, we hypothesize that the intramuscular injection of a red opsin and a blue opsin in opposing muscle pairs enables selective transfection of the nerve fibres corresponding to each compartment such that opposing movements can be produced by changing the illumination wavelength on the mixed nerve. The data presented in this study support this hypothesis. To identify red opsins in the peripheral nervous system, we test a range of promising opsins shown to work in vitro and characterize in vivo peripheral nerve properties and expression longevity. We use ChR2 and CsChrimson to show that spectrally distinct illumination produces opposing muscle movements and electrophysiological recordings specific to the targeted compartment of each opsin. We further explore an optogenetic candidate for spectrally distinct inhibition for the treatment of muscle tremor in peripheral nerves.

We present here a direct cross-comparison of promising opsins in the peripheral nervous system and report that opsin expression

in the peripheral nerve is dependent on intrinsic properties of the opsin. Previous experiments have shown AAV-mediated gene expression in the peripheral nerve is serotype[22], dose[15] and promoter[31] dependent. After controlling for the above, in addition to age of injection and viral concentration, we find that neither Chrimson nor ChrimsonR expresses in the peripheral nervous system as measured histologically or electrophysiologically. We further test ChrimsonR under a varying range of serotypes, dosages, viral sources and injection ages in vivo and find no expression. Previous work has suggested the N-terminus of an ion channel contains a Golgi export signal[32], although modification of this signal in a previous opsin did not yield a change in surface expression[33]. The complete lack of Chrimson expression juxtaposed with the moderate CsChrimson expression therefore implicates the crucial role of this N-terminus in virally mediated peripheral nerve optogenetics. We conclude that N-terminus interaction dynamics with cell trafficking vesicles are critical to peripheral axonal transport and functional axonal expression.

For the opsins that respond within the peripheral nerve, we find that ReaChR is not ideal as judged by lack of wavelength specificity, poor kinetics, low EMG efficiency and short-lived time course of expression. Compared with ReaChR, CsChrimson is found to have greater specificity to red light, higher-amplitude EMG responses, superior high-frequency response and superior time course of expression. However, when evaluating blue light opsins in the peripheral nerve, both CoChR and ChR2 (H134R) outperformed ReaChR and CsChrimson as measured by strength of response and sensitivity. Previous studies have used 100 Hz for tetanized optogenetic contractions[11]. ReaChR is unable to sustain high-frequency stimulation above 5 Hz, which is required for conveying many afferent and efferent biological signals. CsChrimson, however, is able to sustain up to 40 Hz firings, although not consistently. Future work includes the evaluation of CsChrimsonR created by CsChrimson with a K171R mutation; CsChrimsonR combines the membrane targeting N-terminus of CsChrimson with the improved kinetics and redshifted activation of ChrimsonR.

Due to its increased transmittance in biological tissues, the shift from blue to red opsins has been suggested as a critical leap to next stage adoption of optogenetic technologies. The Monte Carlo model suggests that red light reaches two to four times higher fluence rates than blue light at the nerve depths studied within this experiment (1–5 mm). The finding that the sensitivity of CsChrimson in response to transdermal illumination with red light did not outperform the sensitivity of ChR2 in response to transdermal illumination with blue light, even at low illumination intensities, implies that biological processes are a critically important factor in opsin choice and may outweigh benefits conferred by wavelength-dependent absorption and scattering differences. The minimum fluence required to depolarize ChR2 was four times smaller than CoChR, suggesting that the number of functional ChR2 molecules within the axonal membrane must be at least sixteen times greater than the best-expressing CoChR animal, due to CoChR's approximately four times greater photocurrent and more favourable off-kinetics. Histologically, neither CoChR nor CsChrimson expressed as well as ChR2 as measured by overall axon counts. However, total counts are not indicative of illumination sensitivity, which reflects the number of functional opsins per axon. A qualitative assessment shows that the ChR2 axons appear brighter than both CoChR and CsChrimson, which would be consistent with higher opsin concentration per axon. Previous research suggests that the red light photocurrent of CsChrimson is roughly equal to the blue light photocurrent of ChR2(H134R) in vitro[17]. However, because of the difference in minimum fluence required for EMG, we can estimate that CsChrimson must functionally express at approximately eight times lower concentrations within the axonal membrane compared with ChR2.

To test the ability of red light to inhibit deep nerve activity in a spectrally distinct manner, we use Jaws to drive wavelength-dependent inhibition. We show a consistent 40–60% reduction in the magnitude of the muscle electrical activity using Jaws with direct illumination of the nerve. We believe, given high transmittance of red light in tissue, that this level of reduction can be also achieved in a transdermal approach with the use of high-power LEDs operating at low duty cycles to limit heating. The V_{RMS} reduction identified has significant implications for the direct treatment of essential tremor, Parkinson's disease and multiple sclerosis-induced muscle tremor and spasticity. Frequency analyses of both Parkinson's disease and multiple sclerosis-induced tremor have identified 3–8 Hz as the range of tremor encompassing both goal-directed movement and postural activity[34,35]. Here, we show efficacious tremor reduction at 16 Hz, equivalent to harmaline-induced mouse models of essential tremor[36]. Use of spectrally distinct inhibitory opsins would play a significant role during goal-directed movement by enabling alternation of agonist–antagonist muscle inhibition. In the gait cycle, for example, one could inhibit dorsiflexion tremor with red light during toe-off and then inhibit plantarflexion tremor with blue light during terminal swing, both without interfering with voluntary muscle activity. Further, given FES-induced neuroplasticity in paralysis[37], the study of optogenetic tremor inhibition's effect on remodelling motor circuits in the spinal cord and dopaminergic circuits in the brain is of significant scientific interest. Although further work is needed to better understand the time course of tremor reduction, the simplicity and lack of invasiveness of the technique is appealing: one can imagine a targeted muscle injection followed by a small, transdermal LED patch that can be directly controlled by a patient or operated through a feedback loop.

We report muscle atrophy induced by optogenetic transfection of peripheral nerves and discover that atrophy appears correlated to the loss of optogenetic expression. We identify the cause of muscle mass reduction as denervation atrophy, owing to the death of opsin-expressing L3 and L4 ventral horn motor neurons on the ipsilateral side of injection. To rule out direct apoptosis of myocytes, we identify no evidence of inflammation or myocyte death within TA H&E sections. We have previously tested myocytes for ChR2 expression both electrophysiologically (looking for wide spikes) and immunohistochemically, and have found neither, indicating that human synapsin (hSyn) is properly restricting opsin expression to neuronal tissue and that opsin-induced muscle atrophy must be neurogenic[15]. One possible explanation for neuronal cell death is due to direct toxicity of overexpressed opsin molecules resulting in neurogenic apoptosis. Neurogenic apoptosis would result in axonal loss and also explain the low opsin + axon counts in sciatic nerve immunofluorescent cross-sections. As neurons and their corresponding axons die, the previously innervated myocytes will shrink until axonal sprouting results in re-innervation. In this experiment, we identified muscle atrophy and neuronal losses are highest in the opsins that have been the most engineered. The opsins studied here found directly in nature (Chrimson, CoChR) and those with single amino acid substitutions (ChR2 (H134R) and ChrimsonR) had the least atrophy. CsChrimson, which combined two naturally occurring opsins, had moderate atrophy. The opsins, which were heavily engineered (ReaChR and Jaws) had the most atrophy. The engineering of proteins could confer domains that enable higher leakage currents or ion imbalances triggering a neuronal apoptosis-mediated pathway. Another explanation for atrophy is neuronal cell death due to viral, opsin or fluorescent reporter immunogenicity recruiting an adaptive immune response. AAV capsid has been previously shown to result in recruitment of an immune response in a dose-dependent fashion in both previous scientific experiments and human clinical trials[23,24]. However, since AAV serotype and dosage is identical across opsins, it is highly unlikely that AAV immunogenicity alone contributed to atrophy. Because opsins originate

from algae, their DNA may contain CpG motifs that trigger a toll-like receptor 9-mediated innate immune response; alternatively, the protein itself can trigger an adaptive immune response via major histocompatibility complex I presentation. Lastly, excitotoxicity, or light-induced depolarization damage, can also be contributing to neuronal death. We present evidence of ipsilateral inflammation in spinal cord sections, which may occur in the setting of apoptotic or immune-mediated neuronal death. Clinically, researchers looking to treat chronic pain and other peripheral nerve conditions must characterize optogenetic side effects in detail, and offer strategies to combat them. While we believe that the neuronal loss is a solvable challenge, in the event that the neuronal loss remains unsolved, the two-colour strategy still has scientific merit for broad study of the peripheral nervous system including gate-control theory of pain, vagus nerve subtype signalling, motor control and proprioception, and others.

This study proposes a non-invasive wavelength-dependent neurostimulator, which can stimulate nerve fascicles directly by end-organ targeting. We believe that future studies of paralysis, pain, tremor and amputation research may benefit from this work. New studies can employ promoters to restrict spectrally distinct optogenetic transfection to molecularly defined subtypes as opposed to anatomically defined subtypes. The use of $Npy2r^{ChR2}$;$MafA^{ChR2}$ mice have been employed to identify how concurrent low-threshold mechanoreceptor activation alleviates A-fibre mechanonociceptor-evoked pain in a mechanistic study of gate-control pain theory[38]. Within the autonomic nervous system, unique vagal afferent subtypes projecting to the lungs and gastrointestinal tract have been identified to activate different respiratory behaviours and the sensations of satiety, respectively[39,40]. Using a viral construct with conditional expression, one could restrict spectrally distinct opsin to cutaneous or vagal subsets independently. Use of red and blue illumination to study how activation of one axonal subtype alleviates or enhances activation of another would be of significant scientific value for better understanding pain, touch, respiration, satiety and other complex behaviours governed by molecularly distinct opposing subsets of fibres. Stimulation of independent fibres within the same nerve of the same animal alleviates the need for time-intensive development and validation of transgenic strains and allays fears regarding inherent inter-strain variability in physiology experiments. Clinically, the translation of optogenetics in the treatment of human disease is alluring, given the powerful nature of the method and the extremely high incidence of diseases implicated by peripheral nerves. The use of spectrally distinct opsins to stimulate fascicular and fibre groupings of peripheral nerves may play a significant role in the adoption of clinical optogenetic therapies.

Methods

All animal experiments were conducted on Fischer 344 rats under the supervision of the Committee on Animal Care at the Massachusetts Institute of Technology.

Opsin injection. The choice of opsins was based on both a literature search as well as conversations with experts in the field highlighting opsins with promising characteristics in both the red and blue spectra. The construct format was AAV6–hSyn-opsin-reporter-WPRE (woodchuck hepatitis virus posttranscriptional regulatory element). The use of hSyn restricted expression to neural tissue. Virus was produced by Virovek from plasmids at a titre of 1×10^{14} vg ml^{-1} unless otherwise specified. The opsin–fluorescent reporter combinations included ChR2 (H134R)–EYFP[12], CoChR–green fluorescent protein (GP), Chrimson–GFP, ChrimsonR–tdTomato[17], CsChrimson–tdTomato[17], ReaChR–Citrine[16] and Jaws–KGC–GFP–ER2[21], where KGC is Kir 2.1 C terminal export sequence and ER2 is endoplasmic reticulum export signal. Plasmids for CoChR, Chrimson, ReaChR and Jaws were purchased from AddGene. The CsChrimson plasmid was synthesized by Genscript. Under isoflurane anaesthesia, neonatal Fischer 344 rats 2 days postpartum (P2; Charles River Labs) were injected transdermally with 15 µl virus loosely targeting the anterior compartment (Figs. 1a and 6a). The injection was delivered through a 34 G needle (WPI) affixed to an intraocular kit (WPI), Silflex tubing (WPI), and a 10 µl nanofil syringe (WPI) on the UMP3 syringe pump (WPI) with injection rate set to 75 nl s^{-1}. In between each unique virus, the full system was flushed with dH_2O followed by 2% w/v NaOH in dH_2O followed by dH_2O to prevent inter-viral contamination. All 35 rats were housed under a 12:12 light:dark cycle in a temperature-controlled environment with food and water ad libitum and euthanized at 8 weeks post-injection.

Channelrhodopsin electrophysiology measurements. For each channelrhodopsin, a twitch response to both a 473 nm diode-pumped solid-state laser (OptoEngine) and a 635 nm diode laser (OptoEngine) was assessed via transdermal illumination of the lateral right hindlimb of the anaesthetised rat at 2, 4, 6 and 8 weeks post-injection (Fig. 1b). Laser pulses were controlled using a myDAQ (National Instruments) controlled by the NI Elvis Function Generator and custom software written in Matlab. Transdermal illumination targeted two specific locations on the surface of each animal: near the knee for the peroneal nerve and near the mid-calf for the tibial nerve. At 4 and 8 weeks post-injection, direct optogenetic stimulation of the sciatic nerve was also tested for all animals. To stimulate the sciatic nerve directly, a 0.5 cm incision was made on the right lateral hindlimb adjacent to the femur. The knee flexors and extensors were separated via blunt dissection along muscle planes, exposing the sciatic nerve. The presence of a foot twitch in response to illumination was evaluated both electrophysiologically and visually. To measure the strength of the electrophysiological response, four 30G monopolar EMG needles (Natus Medical) were directly inserted through the skin into the GN and TA of each rat for bipolar recording as described previously[15]. Needles were connected to a 20 kS s^{-1} multichannel amplifier with a fixed 200× gain (IntanTech). Both the 473 nm laser and the 635 nm laser were secured above the anaesthetised animal to an assembly allowing for six degrees of freedom. If a twitch was seen visually or electrophysiologically, EMG for each animal was recorded as a function of illumination intensity, frequency, pulse width and molecular fatigue in response to a prolonged stimulation train. Force and EMG were recorded for select trials simultaneously using a force sensor (Shimpo FGV-0.5XY) affixed to the rat foot with suture (Supplementary Fig. 1). Both laser beams had a Gaussian cross-sectional profile and 3 mm diameter ($1/e^2$), corresponding to a peak irradiance at the surface of the skin of 45 mW mm^{-2} at a measured output power of 160 mW. The lasers were verified with a −40 dB CCD (charge-coupled device) and beam profiler software (Thorlabs) to verify the laser beam size, shape and strength were equivalent (Supplementary Fig. 2). Electrical signals controlling the laser amplitude, pulse width and frequency were simultaneously recorded by the amplifier, enabling temporal synchronization of laser pulses and EMG. Two XLamp LEDs (XP-E2, Cree) of 625 nm and 475 nm wavelength were used for transdermal stimulation. LEDs were powered from a current source (T-Cube, ThorLabs) at 1.2 A, 1–5 Hz with 5% duty cycle to limit heating.

Halorhodopsin electrophysiology measurements. For the Jaws rats, the sciatic nerve was exposed at 2, 4, 6 and 8 weeks post-injection as described above. A custom bipolar hook electrode elevated the proximal sciatic nerve. Current pulses (50 µs, 17 Hz, 0.1–4 mA, 5–15 s) stimulated the nerve through the hook electrode while 0.2–1.0 s (17–45 mW mm^{-2}, 20–40% DC) of 473 nm or 635 nm illumination targeted the exposed sciatic nerve, the proximal tibia (transdermal) and the mid-calf (transdermal). During trials, EMG was measured via needle electrodes as described above in both TA and GN channels (Fig. 6b). In a terminal procedure 8 weeks post-injection, the sciatic nerve of the contralateral limb of the 5 rats was exposed and the experiment was repeated as above for the non-injected limb.

Two-opsin injection. To assess selectivity of P2 injections, four P2 pups were injected intramuscularly at 75 nl s^{-1} with 15 µl dye. Two pups were injected with fast green dye (Sigma) in PBS and euthanized immediately afterwards. The other two pups were injected with 0.4% trypan blue (Sigma) and euthanized 24 h later. The injections targeted the hindlimb anterior compartment on the right side and the posterior compartment on the left side. Euthanasia was performed with CO_2 and decapitation. Afterwards, the hindlimb muscles were dissected and photographed (Supplementary Fig. 3). While these dye tests show compartment selectivity, they do not guarantee selectivity for AAV injections. To address this, a fluorescent reporter was used within the AAV construct to identify whether the transduced axons and neurons fall within the subset of axons and neurons corresponding to dorsiflexion (peroneal nerve fascicle + L3 neurons) and plantarflexion (tibial nerve fascicle + L4 neurons).

For the two-opsin viral injections, nine rats were housed under a 12:12 light:dark cycle in a temperature-controlled environment with food and water ad libitum. At P2, six pups were injected intramuscularly with 15 µl AAV6–hSyn–CsChrimson–tdTomato–WPRE targeting the anterior compartment and 15 µl AAV6–hSyn–ChR2 (H134R)–EYFP–WPRE, targeting the posterior compartment. The remaining three pups were injected at P14 under isoflurane anaesthesia. In this procedure, a 0.5 cm incision was made lateral to the mid-tibia. The peroneal nerve was exposed from underneath the biceps femoris and 12 µl of AAV6–hSyn–CsChrimson–tdTomato–WPRE was injected into the exposed anterior compartment adjacent to the peroneal nerve endplate at a rate of 75 nl s^{-1}, and 3 µl was injected directly into the peroneal nerve at the endplate at a rate of 50 nl s^{-1}. The injection system was flushed as described previously and the tibial nerve was exposed. AAV6–hSyn–ChR2 (H134R)–EYFP–WPRE (12 µl) was injected into the

exposed GN adjacent the tibial nerve endplate at a rate of 75 nl s^{-1} and 3 µl was injected into the tibial nerve at the endplate at a rate of 50 nl s^{-1}. The skin incisions were closed with wound clips and wound glue. After 4 weeks and 8 weeks, the P2 rats were tested for responsiveness to both transdermal illumination and direct illumination of the exposed sciatic nerve using both the 473 and 635 nm lasers and the LEDs: three rats were euthanized at each timepoint. During terminal procedures, the peroneal and tibial nerves were exposed by caudal reflection of the biceps femoris muscle and illuminated with both red and blue lasers at varying illumination intensities.

Tissue processing and analysis. Following EMG recordings during terminal procedures, rats were euthanized via intraperitoneal sodium barbital followed by transcardial perfusion with 60 ml PBS followed by 60 ml 4% paraformaldehyde in PBS. Both dorsiflexor and plantarflexor muscle groups on ipsilateral and contralateral hindlimbs were carefully dissected, cut from their origin and insertion points, and weighed. Spinal cord, TA and sciatic nerve were dissected, fixed for 12–24 h, paraffin processed, embedded and cross-sectioned at 10 µm. For the two-opsin animals, spinal cord sections were embedded either longitudinally or in cross-section and sectioned at 10 µm thickness. TA muscle was stained with H&E. Expression of EYFP, GFP and Citrine was amplified with Rb pAb anti-GFP (ab290, Abcam) at 1:200 or Gt pAb anti-GFP (ab5450, Abcam) at 1:100 with anti-Rb Alexa Fluor 488 (Fisher). Expression of tdTomato was amplified with pre-adsorbed Rb pAb anti-red fluorescent protein (600-401-379, Rockland) at 1:25 with anti-Rb Alexa Fluor 568 (Fisher). All antibodies were diluted in 1% w/v BSA in PBS-T. Immunofluorescence images were taken on an Evos FL Auto epifluorescence microscope (Fisher) at ×10 (spinal cord) or ×20 (sciatic nerve). Using ImageJ, opsin$^+$ axons were counted manually whereas total axon counts were estimated from representative counts of subsets of the nerve. Both contralateral and ipsilateral spinal cord neurons were manually counted with ImageJ on H&E stained L3/L4 coronal sections. Assessment of spinal cord inflammation was performed on ×10 ImageJ DAPI+ sections using the freehand selection tool to choose equivalent areas of ventral horn grey matter on left and right coronal lumbar sections. The ImageJ process employed inversion, thresholding, conversion to masks, watershedding, and the 'analyze particles' function with size limits set to 30–250 square pixels per cell. The cell density was determined by dividing the number of cells identified by the area selected; the difference between the ipsilateral cell density and contralateral cell density was reported as a percentage.

Fluence model. To model the fluence rate of red and blue illumination through the rat limb to the nerve, a procedure was used as described previously[15]. Briefly, the right hindlimbs of four 2, 4, 6 and 8-week old Fischer 344 rats were extracted, fixed and sectioned at 10 µm thickness every ~250–500 µm, and stained with H&E. The sciatic nerve was traced to its division into the common peroneal nerve and tibial nerve, which were followed distally to their end plates. The peroneal nerve and tibial nerve depths, relative to skin, was measured on each slice; the slice with the minimum distance between nerve and skin surface was conservatively used for gathering the tissue geometry required for modelling (Supplementary Fig. 4). A Monte Carlo simulation was created in MATLAB for estimating fluence rate distribution in the rat peroneal and tibial nerves using code previously provided[15]. Key inputs to the model included tissue geometry, attenuation coefficients for scattering (μ_s) and absorption (μ_a), and anisotropy factors in skin, muscle, connective tissue, epineurium and nerve, which were gathered from previous studies[41–45]. The model simulated ~10^6 photons, which was sufficient to maintain confidence interval within 5% of fluence estimates using ~10^7 photons. To assess whether stimulation of the nerve was optogenetic in nature and not driven by optically induced heating of the nerve, an optical model of the Pennes bioheat equation was adapted for the peripheral nerve anatomy and tissue properties as described previously[14,46]. In addition to the Monte Carlo output and tissue-specific μ_a, other inputs to the thermal model included tissue density, heat capacity, thermal conductivity, perfusion rate and metabolic generation for rat tissue gathered from the literature (Supplementary Fig. 5)[47–51].

Cell culture. Primary hippocampal cells from Swiss–Webster mice were obtained and cultured as previously published[52]. Cells were incubated with 0.4 ml media containing AAV6 coding for opsin (final concentration: 5E11 vp ml^{-1}) for 72 h. Expression was measured by imaging the fluorescent reporters for each opsin on a confocal fluorescent microscope at ×10 magnification. CellProfiler built-in functions were used to determine the intensity and distribution of expressed opsins within each cell and its axonal projections. Patching of hippocampal cells was performed as described previously[17].

Statistical analysis. Statistical significance was calculated in Microsoft Excel with the data analysis toolbox. For comparisons of individual groups, Student's two-tailed *t*-tests with unequal variance were performed. For comparisons of multiple groups, a single-factor analysis of variance (ANOVA) was performed for significance, followed, if necessary, by post-hoc two-tailed Fishers least significant difference tests for individual groups. All data represent the mean ± s.d. of at least three independent experiments unless otherwise specified; the number of trials is reported in the data provided.

Reporting Summary. Further information on experimental design is available in the Nature Research Reporting Summary linked to this article.

Code availability. The MATLAB.m code used for the temperature simulation, EMG processing and Monte Carlo simulation are available from the corresponding author upon reasonable request.

Data availability. The authors declare that all data supporting the findings of this study are available within the manuscript and its Supplementary information.

Received: 28 June 2017; Accepted: 18 May 2018;
Published online: 25 June 2018

References

1. Navarro, X. et al. A critical review of interfaces with the peripheral nervous system for the control of neuroprostheses and hybrid bionic systems. *J. Peripher. Nerv. Syst.* **10**, 229–258 (2005).
2. Raspopovic, S. et al. Restoring natural sensory feedback in real-time bidirectional hand prostheses. *Sci. Transl. Med.* **6**, 222ra19 (2014).
3. Boretius, T. et al. A transverse intrafascicular multichannel electrode (TIME) to interface with the peripheral nerve. *Biosens. Bioelectron.* **26**, 62–69 (2010).
4. Musick, K. M., Chew, D. J., Fawcett, J. W. & Lacour, S. P. PDMS microchannel regenerative peripheral nerve interface. In *2013 6th International IEEE/EMBS Conference on Neural Engineering (NER)* 649–652 (2013).
5. Maimon, B. et al. Assessment of nerve regeneration through a novel microchannel array. *Int. J. Phys. Med. Rehabil.* **4**, 332 (2016).
6. Dyer, K. R. & Duncan, I. D. The intraneural distribution of myelinated fibres in the equine recurrent laryngeal nerve. *Brain* **110**, 1531–1543 (1987).
7. Stewart, J. D. Peripheral nerve fascicles: anatomy and clinical relevance. *Muscle Nerve* **28**, 525–541 (2003).
8. Thompson, A. C., Stoddart, P. R. & Jansen, E. D. Optical stimulation of neurons. *Curr. Mol. Imaging* **3**, 162–177 (2014).
9. Peterson, E. J. & Tyler, D. J. Motor neuron activation in peripheral nerves using infrared neural stimulation. *J. Neural Eng.* **11**, 16001 (2014).
10. Iyer, S. M. et al. Virally mediated optogenetic excitation and inhibition of pain in freely moving nontransgenic mice. *Nat. Biotechnol.* **32**, 274–278 (2014).
11. Llewellyn, M. E., Thompson, K. R., Deisseroth, K. & Delp, S. L. Orderly recruitment of motor units under optical control in vivo. *Nat. Med.* **16**, 1161–1165 (2010).
12. Towne, C., Montgomery, K. L., Iyer, S. M., Deisseroth, K. & Delp, S. L. Optogenetic control of targeted peripheral axons in freely moving animals. *PLoS ONE* **8**, e72691 (2013).
13. Lin, J. Y. et al. A user's guide to channelrhodopsin variants: features, limitations and future developments. *Exp. Physiol.* **96**, 19–25 (2011).
14. Stujenske, J. M., Spellman, T. & Gordon, J. A. Modeling the spatiotemporal dynamics of light and heat propagation for in vivo optogenetics. *Cell. Rep.* **12**, 525–534 (2015).
15. Maimon, B. et al. Transdermal optogenetic peripheral nerve stimulation. *J. Neural Eng.* **14**, 034002 (2017).
16. Lin, J. Y., Knutsen, P. M., Muller, A., Kleinfeld, D. & Tsien, R. Y. ReaChR: a red-shifted variant of channelrhodopsin enables deep transcranial optogenetic excitation. *Nat. Neurosci.* **16**, 1499–1508 (2013).
17. Klapoetke, N. C. et al. Independent optical excitation of distinct neural populations. *Nat. Methods* **11**, 338–346 (2014).
18. Fenno, L., Yizhar, O., & Deisseroth, K. The development and application of optogenetics. *Annu. Rev. Neurosci.* **34**, 389–412 (2011).
19. Prigge, M. et al. Color-tuned channelrhodopsins for multiwavelength optogenetics. *J. Biol. Chem.* **287**, 31804–31812 (2012).
20. Lin, J. Y., Lin, M. Z., Steinbach, P. & Tsien, R. Y. Characterization of engineered channelrhodopsin variants with improved properties and kinetics. *Biophys. J.* **96**, 1803–1814 (2009).
21. Chuong, A. S. et al. Noninvasive optical inhibition with a red-shifted microbial rhodopsin. *Nat. Neurosci.* **17**, 1123–1129 (2014).
22. Mason, M. R. et al. Comparison of AAV serotypes for gene delivery to dorsal root ganglion neurons. *Mol. Ther.* **18**, 715–724 (2010).
23. Hareendran, S. et al. Adeno-associated virus (AAV) vectors in gene therapy: immune challenges and strategies to circumvent them. *Rev. Med. Virol.* **23**, 399–413 (2013).
24. Mingozzi, F. et al. Immune responses to AAV vectors: overcoming barriers to successful gene therapy. *Blood* **122**, 23–36 (2013).
25. Wang, H. et al. High-speed mapping of synaptic connectivity using photostimulation in channelrhodopsin-2 transgenic mice. *Proc. Natl Acad. Sci. USA* **104**, 8143–8148 (2007).
26. Zepetnek, J. E. T., de Gordon, T., Stein, R. B. & Zung, H. V. Comparison of force and EMG measures in normal and reinnervated tibialis anterior muscles of the rat. *Can. J. Physiol. Pharmacol.* **69**, 1774–1783 (1991).

27. Schmalbruch, H. Fiber composition of the rat sciatic nerve. *Anat. Rec.* **215**, 71–81 (1986).
28. Mense, S. Muscle pain: mechanisms and clinical significance. *Dtsch Arztebl. Int.* **105**, 214–219 (2008).
29. Mohan, R., Tosolini, A. P. & Morris, R. Targeting the motor end plates in the mouse hindlimb gives access to a greater number of spinal cord motor neurons: an approach to maximize retrograde transport. *Neuroscience* **274**, 318–330 (2014).
30. Tozburun, S., Cilip, C. M., Lagoda, G. A., Burnett, A. L. & Fried, N. M. Continuous-wave infrared optical nerve stimulation for potential diagnostic applications. *J. Biomed. Opt.* **15**, 55012 (2010).
31. Gray, S. J. et al. Optimizing promoters for recombinant adeno-associated virus-mediated gene expression in the peripheral and central nervous system using self-complementary vectors. *Hum. Gene Ther.* **22**, 1143–1153 (2011).
32. Hofherr, A., Fakler, B. & Klöcker, N. Selective Golgi export of Kir2.1 controls the stoichiometry of functional Kir2.x channel heteromers. *J. Cell. Sci.* **118**, 1935–1943 (2005).
33. Gradinaru, V. et al. Molecular and cellular approaches for diversifying and extending optogenetics. *Cell* **141**, 154–165 (2010).
34. Alusi, S. H., Glickman, S., Aziz, T. Z. & Bain, P. G. Tremor in multiple sclerosis. *J. Neurol. Neurosurg. Psychiatry* **66**, 131–134 (1999).
35. O'Suilleabhain, P. E. & Matsumoto, J. Y. Time-frequency analysis of tremors. *Brain* **121**, 2127–2134 (1998).
36. Harmaline induced tremors. *PsychoGenics* http://www.psychogenics.com/harmaline.html (accessed 2 June 2017).
37. McGie, S. C., Zariffa, J., Popovic, M. R. & Nagai, M. K. Short-term neuroplastic effects of brain-controlled and muscle-controlled electrical stimulation. *Neuromodulation Technol. Neural Interface* **18**, 233–240 (2015).
38. Arcourt, A. et al. Touch receptor-derived sensory information alleviates acute pain signaling and fine-tunes nociceptive reflex coordination. *Neuron* **93**, 179–193 (2017).
39. Williams, E. K. et al. Sensory neurons that detect stretch and nutrients in the digestive system. *Cell* **166**, 209–221 (2016).
40. Chang, R. B., Strochlic, D. E., Williams, E. K., Umans, B. D. & Liberles, S. D. Vagal sensory neuron subtypes that differentially control breathing. *Cell* **161**, 622–633 (2015).
41. Bashkatov, A. N. et al. In vivo and in vitro study of control of rat skin optical properties by acting of osmotical liquid. *Biomed. Photon. Optoelectronic Imaging* **4224**, 300–311 (2000).
42. Bashkatov, A. N., Genina, E. A. & Tuchin, V. V. Optical properties of skin, subcutaneous, and muscle tissues: a review. *J. Innov. Opt. Health Sci.* **4**, 9–38 (2011).
43. Islam, M. S. et al. Extracting structural features of rat sciatic nerve using polarization-sensitive spectral domain optical coherence tomography. *J. Biomed. Opt.* **17**, 56012 (2012).
44. Hendriks, B. H. W. et al. Nerve detection with optical spectroscopy for regional anesthesia procedures. *J. Transl. Med.* **13**, 380 (2015).
45. Yaroslavsky, A. N. et al. Optical properties of selected native and coagulated human brain tissues in vitro in the visible and near infrared spectral range. *Phys. Med. Biol.* **47**, 2059 (2002).
46. Pennes, H. H. Analysis of tissue and arterial blood temperatures in the resting human forearm. *J. Appl. Physiol.* **1**, 93–122 (1948).
47. Ward, S. R. & Lieber, R. L. Density and hydration of fresh and fixed human skeletal muscle. *J. Biomech.* **38**, 2317–2320 (2005).
48. Hasgall, P. et al. *IT'IS Database for Thermal and Electromagnetic Parameters of Biological Tissues* Version 3.0 (IT'IS Foundation, 2015); https://doi.org/10.13099/VIP21000-03-0
49. Fagher, B. & Monti, M. Thermogenic effect of two β-adrenoceptor blocking drugs, propranolol and carvedilol, on skeletal muscle in rats. A microcalorimetric study. *Thermochim. Acta* **251**, 183–189 (1995).
50. Allen, J. T., Allen, J. T. & Bowman, H. F. The simultaneous measurement of thermal conductivity, thermal diffusivity, and perfusion in small volumes of tissue. *J. Biomech. Eng.* **106**, 192 (1984).
51. Rins, M., Diez, I., Calpena, A. C., & Obach, R. Skin density in the hairless rat. Evidence of regional differences. *Eur. J. Drug. Metab. Pharmacokinet.* **Spec. No. 3**, 456–457 (1991).
52. Boyden, E. S., Zhang, F., Bamberg, E., Nagel, G. & Deisseroth, K. Millisecond-timescale, genetically targeted optical control of neural activity. *Nat. Neurosci.* **8**, 1263–1268 (2005).

Acknowledgements

We thank C. Towne for his assistance in crafting the motivation for this project. We thank E. Boyden for his assistance and consultation on this project. Furthermore, we thank K. Cormier, C. Condon, M. Brown, as well as the entire Koch Histology Core for their countless hours of painstaking histology efforts. In addition, we thank N. Klapoetke, O. Shemesh, K. Piatkevich, E. Revol, P. Calvaresi, C. Varela, A. Harding, M. Fahmi, C. Lee, H.-J. Suk, D. Park, M. Diaz, A. Schneider and S. Osseiran for their advice, guidance and assistance. This work was funded by the MIT Media Lab Consortium.

Author contributions

B.E.M. and H.M.H. contributed to idea conception, study design and data analysis. B.E.M. oversaw experiment conduction and data analysis for in vivo experiments including histology and fluence modelling. K.S. contributed to experiment conduction, data collection and histology processing. S.S. performed in vitro screen experiments along with corresponding data processing. A.N.Z. contributed to idea conception and experiment planning as well as assisted with Monte Carlo modelling. B.E.M. wrote the manuscript with all authors contributing to editing the text.

Competing interests

The authors declare no competing interests.

Additional information

Supplementary information is available for this paper at https://doi.org/10.1038/s41551-018-0255-5.

Reprints and permissions information is available at www.nature.com/reprints.

Correspondence and requests for materials should be addressed to H.M.H.

Publisher's note: Springer Nature remains neutral with regard to jurisdictional claims in published maps and institutional affiliations.

nature research

Corresponding author(s): Hugh Herr, Benjamin Maimon

Life Sciences Reporting Summary

Nature Research wishes to improve the reproducibility of the work that we publish. This form is intended for publication with all accepted life science papers and provides structure for consistency and transparency in reporting. Every life science submission will use this form; some list items might not apply to an individual manuscript, but all fields must be completed for clarity.

For further information on the points included in this form, see Reporting Life Sciences Research. For further information on Nature Research policies, including our data availability policy, see Authors & Referees and the Editorial Policy Checklist.

Please do not complete any field with "not applicable" or n/a. Refer to the help text for what text to use if an item is not relevant to your study.
For final submission: please carefully check your responses for accuracy; you will not be able to make changes later.

Experimental design

1. Sample size

Describe how sample size was determined.

Sample sizes were predetermined using the formula for continuous variables based on prior EMG data for inter-group variability in a peripheral nerve EMG ChR2-only dosage test. This suggested that a sample size of 4.5 was required. For two-color animals, sample size was chosen to be 9.

2. Data exclusions

Describe any data exclusions.

No data were excluded from the experiment.

3. Replication

Describe the measures taken to verify the reproducibility of the experimental findings.

All attempts at replication were successful.

4. Randomization

Describe how samples/organisms/participants were allocated into experimental groups.

Groups were determined by litter. Each group represented a mother with a litter of 5 rats. Since Fisher 344 rats are an inbred strain, no significant genetic variation will be present from one group to another.

5. Blinding

Describe whether the investigators were blinded to group allocation during data collection and/or analysis.

Blinding was not performed during data collection because no subjective metrics were measured or reported. However, blinding was performed during immunofluorescence image analysis to verify that no bias was introduced during manual axon counting.

Note: all in vivo studies must report how sample size was determined and whether blinding and randomization were used.

6. Statistical parameters

For all figures and tables that use statistical methods, confirm that the following items are present in relevant figure legends (or in the Methods section if additional space is needed).

n/a	Confirmed
☐	☒ The exact sample size (*n*) for each experimental group/condition, given as a discrete number and unit of measurement (animals, litters, cultures, etc.)
☐	☒ A description of how samples were collected, noting whether measurements were taken from distinct samples or whether the same sample was measured repeatedly
☐	☒ A statement indicating how many times each experiment was replicated
☐	☒ The statistical test(s) used and whether they are one- or two-sided *Only common tests should be described solely by name; describe more complex techniques in the Methods section.*
☐	☒ A description of any assumptions or corrections, such as an adjustment for multiple comparisons
☐	☒ Test values indicating whether an effect is present *Provide confidence intervals or give results of significance tests (e.g. P values) as exact values whenever appropriate and with effect sizes noted.*
☐	☒ A clear description of statistics including central tendency (e.g. median, mean) and variation (e.g. standard deviation, interquartile range)
☐	☒ Clearly defined error bars in all relevant figure captions (with explicit mention of central tendency and variation)

See the web collection on statistics for biologists for further resources and guidance.

Software

Policy information about availability of computer code

7. Software

Describe the software used to analyze the data in this study.	Matlab R2014B was used to analyze and process EMG data into VRMS values. Microsoft Excel was used to compile, find statistics of data, and plot data. ImageJ and CellProfiler were used to analyze immunofluorescence and in vitro cell fluorescence images, respectively.

For manuscripts utilizing custom algorithms or software that are central to the paper but not yet described in the published literature, software must be made available to editors and reviewers upon request. We strongly encourage code deposition in a community repository (e.g. GitHub). *Nature Methods* guidance for providing algorithms and software for publication provides further information on this topic.

Materials and reagents

Policy information about availability of materials

8. Materials availability

Indicate whether there are restrictions on availability of unique materials or if these materials are only available for distribution by a third party.	There are no restrictions on the availability of unique materials.

9. Antibodies

Describe the antibodies used and how they were validated for use in the system under study (i.e. assay and species).	Expression of EYFP, GFP, and Citrine was amplified with Rb pAb anti-GFP (ab290, Abcam) at 1:200 or Gt pAb anti-GFP (ab5450, Abcam) at 1:100 with anti-Rb Alexa Fluor 488 (Fisher). Expression of tdtomato was amplified with pre-adsorbed Rb pAb anti-RFP (600-401-379, Rockland) at 1:25 with anti-Rb Alexa Fluor 568 (Fisher). All antibodies were diluted in 1% w/v BSA in PBS-T. Ab290 was validated in a previous work for ChR2 peripheral axons using a dilution curve. Ab5450 was validated against ab290 also with a dilution curve and a negative control non-expressing nerve tissue. The Rockland anti-RFP used above was tested against 5 other anti-RFP antibodies at manufacturer recommended dilutions: Biorbyt orb182397, Origene TA150129, LSBio LS-C340696, Abcam ab65856, and Abcam ab62341. We discovered that all polyclonal antibodies, with the exception of the Rockland antibody, resulted in non-specific staining to Schwann cells in negative control experiments and false positives when performing axon counts. The one monoclonal antibody (ab65856) did not recognize the RFP protein, likely due to paraformaldehyde and ethanol quenching of native protein structure during paraffin processing tissue preparation. Rockland anti-RFP was purchased because it is pre-adsorbed, and likely as a result, it had no noticeable schwann cell non-specific staining. After discovering this antibody also robustly recognized csChrimson-tdtomato, it was used for all further immunofluorescence imaging. For double immunostaining, each nerve sample was stained independently to determine appropriate dilution, and then nerves were stained together with goat anti-GFP and rabbit anti-RFP with corresponding 488 and 568 secondaries. Both total axon counts and axon location within the nerve matched between the single and double images. To verify that counting was appropriately recognizing opsin+ axons, counting was performed for each nerve fiber manually. This allowed us to control for elements of dirt, autofluorescence, or non-specific staining of schwann cells, that otherwise had interfered with automated processing algorithms we had attempted to employ.

10. Eukaryotic cell lines

a. State the source of each eukaryotic cell line used.	No eukaryotic cell lines were used. Hippocampal cells were primary.
b. Describe the method of cell line authentication used.	No eukaryotic cell lines were used.
c. Report whether the cell lines were tested for mycoplasma contamination.	No eukaryotic cell lines were used
d. If any of the cell lines used are listed in the database of commonly misidentified cell lines maintained by ICLAC, provide a scientific rationale for their use.	No commonly misidentified cell lines were used.

Animals and human research participants

Policy information about studies involving animals; when reporting animal research, follow the ARRIVE guidelines

11. Description of research animals

Provide all relevant details on animals and/or animal-derived materials used in the study.

Seven Fischer 344 rats mother with 5-male litter at P2 were purchased from Charles River Labs. Viral injections occurred on same day as animal arrival. Animals were weaned at 24 days of age. For two color rats, three Fischer 344 mother with litter rats were purchased from Charles River Labs. Animals were injected at P2 or P14 as specified in the manuscript.

Policy information about studies involving human research participants

12. Description of human research participants

Describe the covariate-relevant population characteristics of the human research participants.

The study did not involve human research participants.